THE ROLE OF ICE COMPOSITIONS AND MORPHOLOGY FOR SNOWLINES AND THE C/N/O RATIOS IN ACTIVE DISKS

Ana-Maria A. Piso[1], Karin I. Öberg[1], Jamila Pegues[2]
Draft version January 24, 2016

ABSTRACT

The elemental compositions of planets define their chemistry, and could potentially be used as beacons for their formation location if the elemental gas and grain ratios of planet birth environments, i.e. protoplanetary disks, are well understood. In disks, the ratios of volatile elements, such as C/O and N/O, are regulated by the abundance of the main C, N, O carriers, the ice environment in which these carriers reside, and the presence of snowlines of major volatiles at different distances from the central star. We explore the effects of dynamical processes, molecular compositions and abundances, and the ice morphology of dust grains in disks on the snowline locations of the main C, O and N carriers, and their consequences for the C/N/O ratio in gas and dust throughout the disk. We find that radial drift and accretion alone can reduce the snowline radii of the main C, O and N carriers, i.e. H_2O, CO_2, CO and N_2, by 40-60% compared to static disks. If CO and N_2 are bound to water ice instead of pure ices, their snowlines move inward by $\sim$70%. Both of these effects substantially change the disk regions where C/O and N/O are enhanced over the stellar value. In the outer disk, the gaseous C/O and N/O are enhanced by factors of $\sim$2 and $\sim$3, respectively. Our estimates for the C/N/O ratios are only modestly affected by the presence of some C in the form of CH_4 and of some N in the form of NH_3.

1. INTRODUCTION

•

Background info. Importance of volatiles in disks and planetary atmospheres, detections of snowlines in disks, C/O ratios etc. State again the importance of radial drift and gas accretion on the snowline locations, and that a systematic study of the combination of these two particular effects across the disk has not been done before. Then transition to the fact that we provide such a systematic study in Paper I and in this paper. Here, we expand the model of Paper I by making three additions: (1) we add N and CH4 in the static chemistry model, and explore how different abundances of CH4 and of the N main carriers (N2 and NH3) affect the C/O and N/O ratios, (2) we quantify the effect of radial drift and gas accretion on the N2, CH4 and NH3 snowline locations, and (3) we explore how different binding energies of CO and N2 affect their snowline locations.

2. COUPLED DRIFT-DESORPTION MODEL REVIEW

We begin with a brief review of Paper I's model for the effect of radial drift and viscous gas accretion on volatile snowline locations. We review our disk model in Section 2.1, and summarize our numerical method and results in Section 2.2.

2.1. *Disk Model*

We first assume a static disk, which is only irradiated by the central star and does not experience redistribution of solids or radial movement of the nebular gas. To quantify the effects of radial drift and gas accretion, we

[1] Harvard-Smithsonian Center for Astrophysics, 60 Garden Street, Cambridge, MA 02138
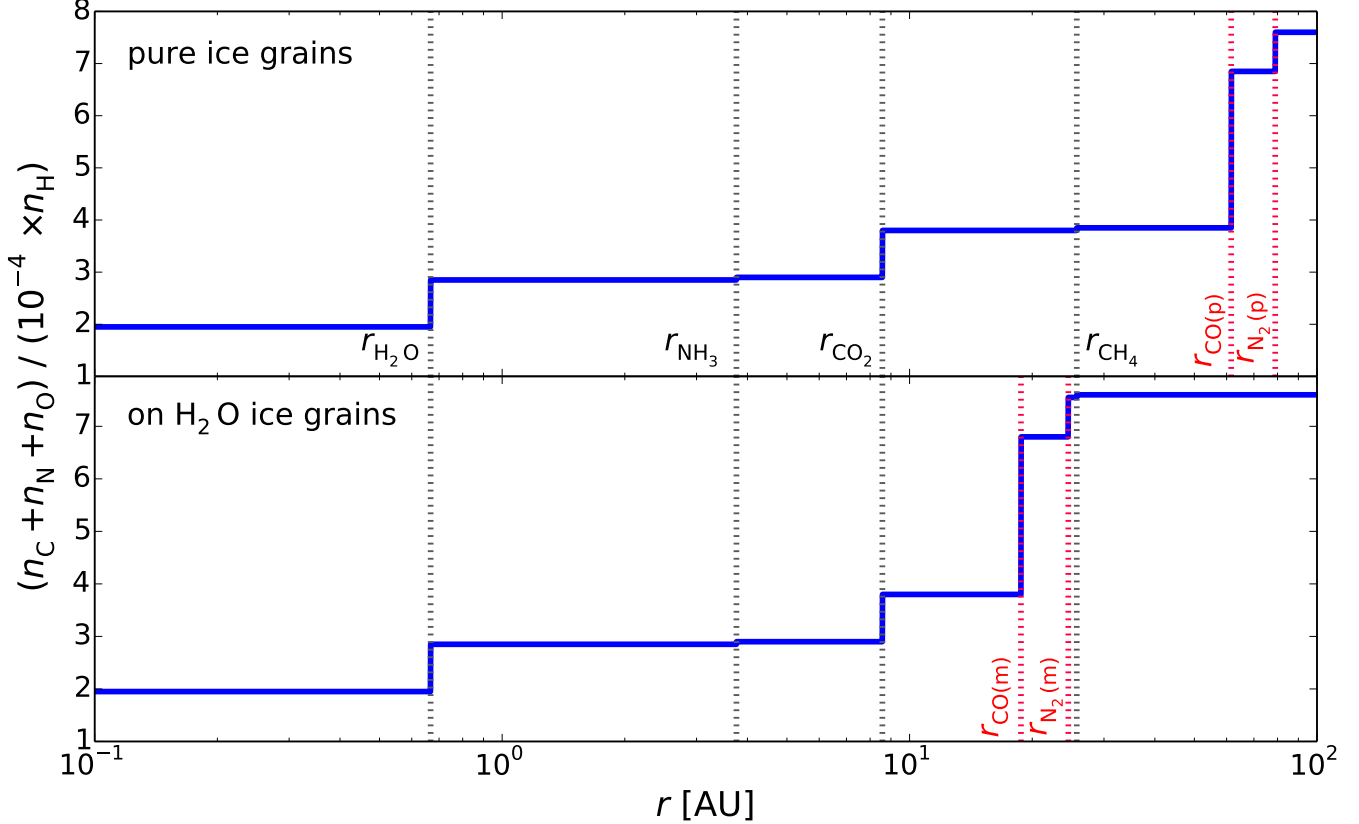[2] Department of Astrophysical Sciences, Princeton University

use a viscous disk with a spatially and temporally constant mass flux, $\dot{M}$. The viscous disk takes into account radial drift, gas accretion onto the central star, as well as accretion heating. We prefer this disk model to an irradiated or evolving disk (see Paper I) because it includes all the dynamical and thermal processes we are interested in for the scope of this paper, and therefore it is the most realistic one.

Following Chiang & Youdin (2010), the temperature profile for a static disk is

$$T = 120\,(r/\mathrm{AU})^{-3/7}\ \mathrm{K}, \qquad (1)$$

where r is the semimajor axis. We use the Shakura & Sunyaev (1973) steady-state disk solution to model the viscous disk. From Paper I, the viscous disk temperature profile is computed as

$$T_{\mathrm{act}} = \frac{1}{4r}\left(\frac{3G\kappa_0 \dot{M}^2 M_* \mu m_{\mathrm{p}} \Omega_{\mathrm{k}}}{\pi^2 \alpha k_{\mathrm{B}} \sigma}\right)^{1/3}. \qquad (2)$$

Here G is the gravitational constant, $\kappa_0 = 2 \times 10^{-6}$ is a dimensionless coefficient in the opacity law $\kappa = \kappa_0 T_{\mathrm{act}}^2$, $M_* = M_\odot$ is the mass of the central star, $\mu = 2.35$ is the mean molecular weight of the nebular gas, m_{p} is the proton mass, $\Omega_{\mathrm{k}} = \sqrt{GM_\odot/r^3}$ is the Keplerian angular velocity, $\alpha = 0.01$ is a dimensionless coefficient (see below for details), k_{B} is the Boltzmann constant, and σ is the Stefan-Boltzmann constant. The final midplane temperature profile is computed as

$$T^4 = T_{\mathrm{act}}^4 + T_{\mathrm{irr}}^4, \qquad (3)$$

where $T_{\mathrm{irr}} = T$ from Equation (1). We use this expression because in addition to accretion heating, stellar irradiation also contributes to the disk thermal structure.

The steady-state disk has an α-viscosity prescription, where the kinematic viscosity is $\mu = \alpha c H$. Here $c \equiv$

FIG. 1.— CNO abundance in grains...

$\sqrt{k_{\mathrm{B}}T/(\mu m_{\mathrm{p}})}$ is the isothermal sound speed (with T from Equation 3), and $H \equiv c/\Omega_{\mathrm{k}}$ is the disk scale height. We can then determine the gas surface density for a viscous disk as (Shakura & Sunyaev 1973; see also Paper I for a more detailed explanation of these calculations):

$$\Sigma = \frac{\dot{M}}{3\pi\nu}. \qquad (4)$$

We choose $\dot{M} = 10^{-8}M_{\odot}$ yr^{-1}, consistent with mass flux observations in disks (e.g., Andrews et al. 2010). As acknowledged in Paper I, the mass flux rate $\dot{M}$ and stellar luminosity L_* will vary throughout the disk lifetime (Kennedy et al. 2006, Chambers 2009), in contrast with our simplified model which assumes that both quantities are constant. This effect will be most pronounced in the inner disk ($\lesssim$ few AU), where accretion heating dominates. We thus acknowledge that the location of the H$_2$O snowline may be determined by the decline in $\dot{M}$ or L_* with time, rather than radial drift (see Paper I, Section 2.1 for a more detailed explanation).

2.2. *Desorption-Drift Equations and Results*

For a range of initial icy grain sizes composed of a single volatile, we showed in Paper I that the timescale on which these particles desorb is comparable to their radial drift time, as well as to the accretion timescale of the nebular gas onto the central star. We thus have to take into account both drift and gas accretion when we

calculate the disk location at which a particle desorbs, since that location may be different from the snowline position in a static disk for a given volatile (see Figure 1 and Öberg et al. 2011b). We determine a particle's final location in the disk by solving the following coupled differential equations:

$$\frac{ds}{dt} = -\frac{3\mu_x m_{\mathrm{p}}}{\rho_{\mathrm{s}}} N_x R_{\mathrm{des,x}} \qquad (5a)$$

$$\frac{dr}{dt} = \dot{r}, \qquad (5b)$$

where s is the particle size, t is time, μ_x is the mean molecular weight of volatile x, $\rho_{\mathrm{s}} = 2$ g cm^{-3} is the density of an icy particle, $N_x \approx 10^{15}$ sites cm^{-2} is the number of adsorption sites of molecule x per cm^{-2}, $R_{\mathrm{des,x}}$ is the desorption rate of species x, and $\dot{r}$ is the particle's radial drift velocity. We calculate $R_{\mathrm{,des}}$ and $\dot{r}$ as follows.

The desorption rate $R_{\mathrm{des,x}}$ (per molecule) is (Hollenbach et al. 2009)

$$R_{\mathrm{des,x}} = \nu_x \exp\left(-E_x/T_{\mathrm{grain}}\right), \qquad (6)$$

where E_x is the adsorption binding energy in units of Kelvin, $T_{\mathrm{grain}} = T$ is the grain temperature (assumed to be the same as the disk temperature, see Paper I), and $\nu_x = 1.6 \times 10^{11}\sqrt{(E_x/\mu_x)}$ s^{-1} is the molecule's vibrational frequency in the surface potential well. We discuss our choices for E_x for the different volatile species in Sections 3 and 4.

Following Chiang & Youdin (2010) and Birnstiel et al. (2012), a particle's radial drift velocity can be approximated as

$$\dot{r} \approx -2\eta\Omega_{\mathrm{k}}r\left(\frac{\tau_{\mathrm{s}}}{1+\tau_{\mathrm{s}}^2}\right) + \frac{\dot{r}_{\mathrm{gas}}}{1+\tau_{\mathrm{s}}^2}, \qquad (7)$$

where the first term is the drift velocity in a non-accreting disk and the second term accounts for the radial movement of the gas. Here $\eta \approx c^2/(2v_{\mathrm{k}}^2)$, where v_{k} is the Keplerian velocity, and $\tau_{\mathrm{s}} \equiv \Omega_{\mathrm{k}}t_{\mathrm{s}}$ is the dimensionless stopping time:

$$t_{\mathrm{s}} = \begin{cases} \rho_{\mathrm{s}}s/(\rho c), & s < 9\lambda/4 \quad \text{Epstein drag} \\ 4\rho_{\mathrm{s}}s^2/(9\rho c\lambda), & s < 9\lambda/4,\ \mathrm{Re} \lesssim 1 \quad \text{Stokes drag}, \end{cases} \qquad (8)$$

where ρ is the disk mid-plane density, λ is the mean free path and Re is the Reynolds number. The gas accretion velocity $\dot{r}_{\mathrm{gas}}$ is determined from $\dot{M} = -2\pi r\dot{r}_{\mathrm{gas}}\Sigma$, for a fixed $\dot{M}$ and with Σ given by Equation (4).

For a particle of initial size s_0, we solve the Equation set (5) with the initial conditions $s(t_0) = s_0$ and $r(t_0) = r_0$, where t_0 is the time at which we start the integration and r_0 is the particle's initial location. We stop our simulation after $t_{\mathrm{d}} = 3$ Myr, the disk lifetime, since this is roughly the timescale on which planets form (), and determine the desorption timescale t_{des} from $s(t_{\mathrm{des}}) = 0$, and thus a particle's desorption distance $r_{\mathrm{des}} = r(t_{\mathrm{des}})$. Our results are insensitive to our choice of t_0 as long as $t_0 \ll t_{\mathrm{d}}$. We note that a particle's size is initially fixed and only changes due to desorption. We thus do not take into account processes such as grain coagulation or fragmentation, which nonetheless occur in disks (e.g., Birnstiel et al. 2012, Pérez et al. 2012). We discuss the effect of these processes on snowline locations in Paper I.

As we show in Paper I, a particle of initial size s_0 can experience three outcomes after $t_{\mathrm{d}} = 3$ Myr: (1) it can remain at its initial location, (2) it can drift towards the host star, then stop without evaporating significantly, and (3) it can completely desorb on a timescale shorter than 3 Myr. Particles in scenarios (1) and (2) are thus not affected by radial drift or gas accretion, and the snowline locations are those for a static disk. In contrast, the grains in case (3) desorb *instantaneously* and *at a fixed particle-size dependent location* in the disk, regardless of their initial position. The snowline locations for these particles will thus be fixed for a given initial particle size and disk model. We have found that grains with sizes ~ 0.001 cm $\lesssim s \lesssim 7$ satisfy this condition for our fiducial disk.

3. CH$_4$ AND C/O RATIOS

Both in Solar system comets and in protoplanetary disks, carbon and oxygen are primarily contained in H_2O, CO_2 and CO (e.g., Rodgers & Charnley 2002, Lodders 2003, Pontoppidan 2006). However, some fraction of the carbon abundance may also be carried by CH_4 (e.g., Mumma et al. 1996), which may change the C/O ratio in gas and in dust throughout the disk. To quantify the magnitude of this effect, we use measured CH_4 abundances in protostellar cores from the *Spitzer* c2d Legacy ice survey (Evans et al. 2003). We explore the parameter space of possible CH_4 abundances by assum-

ing three different scenarios: (1) no CH_4, (2) the median CH_4 observed abundance (hereafter CH_4-mid), and (3) the maximum CH_4 observed abundance (hereafter CH_4-max). Thus $n_{CH_4-mid} = 0.0555 \times n_{H_2O}$ (Öberg et al. 2011a) and $n_{CH_4-mid} = 0.13 \times n_{H_2O}$ (Öberg et al. 2008). Similarly to Paper I, we use the H_2O, CO_2 and CO abundances of Öberg et al. (2011b). Since the abundance of carbon grains is uncertain, we assume that all the carbon that is not in the form of CH_4 is found in carbon grains, so that we reproduce the Solar C/O ratio (gas+dust) of 0.54.

We determine the location of the H_2O, CO_2, CO and CH_4 snowlines in our static disk by balancing desorption with readsorption, following Hollenbach et al. (2009). The binding energies of H_2O, CO_2, CO and CH_4 as pure ices are 5800 K, 2000 K, 834 K and 1300 K, respectively (Fraser et al. 2001, Collings et al. 2004, Fayolle et al. 2016, Garrod & Herbst 2006).
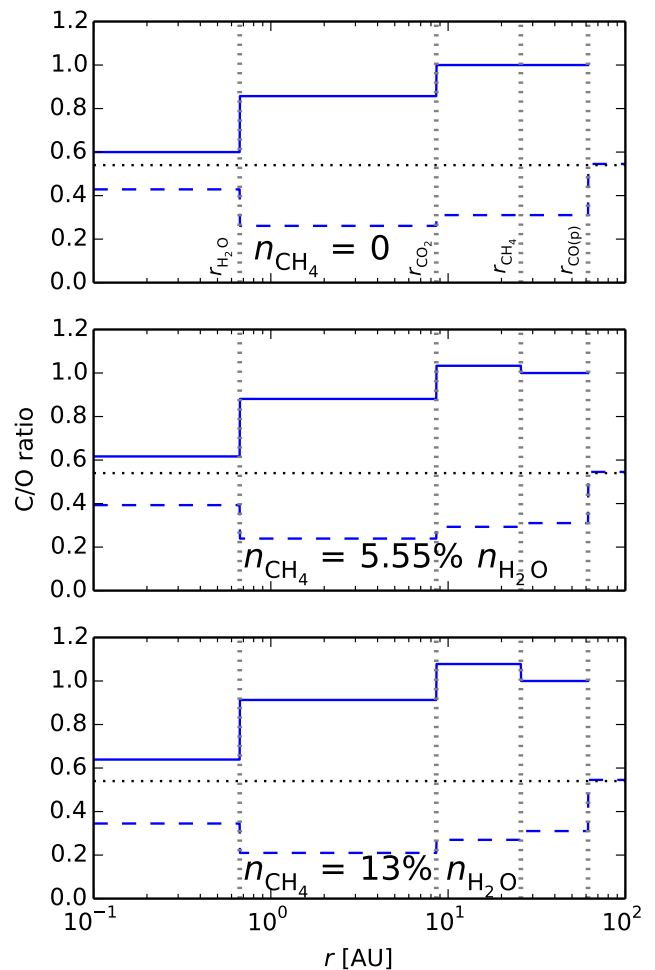

FIG. 2.— C/O ratio in a static disk for different CH4 abundances and CO binding energies...

Figure 2 shows the C/O ratio in gas and dust as a function of semimajor axis in a static disk, for different CH_4 abundances as outlined above. As in Öberg et al. (2011b) and Paper I, a gaseous C/O ratio of unity can

be achieved beyond the CO_2 snowline, where oxygen gas is significantly depleted (top panel). The gas-phase C/O ratio may be further enhanced between the CO_2 and CH_4 snowlines due to the presence of additional carbon gas from CH_4. In this region, the C/O ratio increases by 3% for CH_4-mid and by 8% for CH_4-max, as displayed in the middle and bottom panel of Figure 2. Based on current observations of CH_4 abundances, its presence in the disk only modestly affects the C/O ratio. Given the larger uncertainties in overall volatile abundances, we can neglect CH_4 when estimating the C/O ratio in static disks

As noted in Section 1, the CO binding energy varies significantly depending on the environment in which the icy grains reside. If CO ice is layered on top of a water ice substrate, its binding energy will be larger than in the pure ice case (834 K) due to the higher H_2O binding energy. Fayolle et al. (2016) find a CO binding energy of 1388 K in the layered ice scenario. We use the model of Section 2 to estimate the movement of the CO snowline for different grain morphologies in a viscous disk.

Figure 3 shows the H_2O, CO_2 and CO snowline locations for particles with initial sizes ~ 0.06 cm $\lesssim s \lesssim 7$ m as well as estimates for the C/O ratio in gas and dust in a viscous disk, with the CO snowline calculated under different grain morphologies as noted above. The true snowline for particles that desorb outside the static snowline is the static snowline itself, hence desorbing particles with $s < 0.06$ cm do not form true snowlines. As calculated in Paper I, drift and gas accretion may move the snowlines inwards by up to 40-60% compared to a static disk, and specifically by up to ~ 50 % in the case of the CO snowline. This result is preserved for the updated CO binding energies, both for pure ice and on a water ice substrate. However, a layered grain structure moves the CO snowline inwards significantly: for our fiducial disk model, $r_{CO,layered} \approx 8.7$ AU. Thus if CO is bound to water ice instead of pure ices, the CO snowline may move inward by up to 70%. This large inward movement of the CO snowline implies that C/O ratios of order unity may be reached much closer to the host star if CO is layered on a water ice substrate, and may be inside 10 AU for certain disk parameters.

4. NITROGEN AND N/O RATIOS

In addition to carbon and oxygen, nitrogen is another abundant volatile in the Solar system and in disks. Chemical models of the protostellar nebula (e.g., Owen et al. 2001) and of protoplanetary disks (e.g., Rodgers & Charnley 2002) suggest that N_2 was the dominant form of nitrogen, and that giant planets have accreted their nitrogen content primarily as N_2 (Mousis et al. 2014). Observations of Solar system bodies such as Titan and Pluto show that N_2 is prevalent in their atmospheres (Cruikshank et al. 1993, Owen et al. 1993). Moreover, the Rosetta spacecraft has recently made the first direct measurement of N_2 abundance in comet 67P/Churyumov-Gerasimenko (Rubin et al. 2015). In addition to N_2, a fraction of the nitrogen abundances may be also carried by NH_3 (Bottinelli et al. 2010, Mumma & Charnley 2011).

Because of the high volatility of N_2, the gas phase nitrogen-to-oxygen (N/O) ratio in the outer disk may be even more enhanced than the C/O ratio compared to its average value in the disk. Giant planets that form
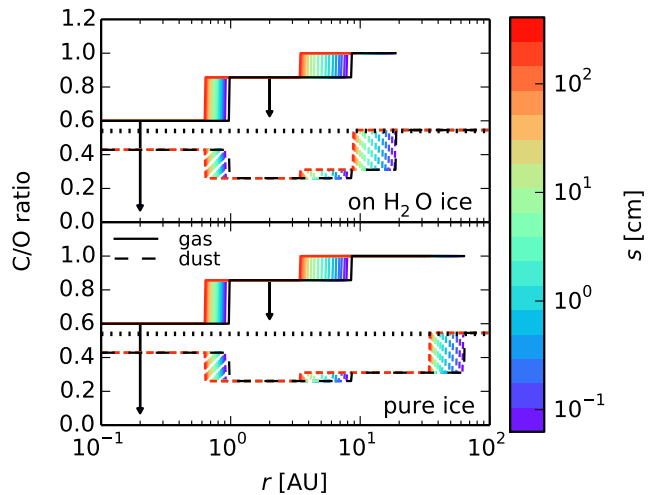

FIG. 3.— C/O ratio as function of semimajor axis for CO combined with H2O (top panel) and pure CO ice (bottom panel).... Drift and gas accretion move the CO snowlines inward by x% and y%, respectively.

at wide separations should thus have an excess of nitrogen in their atmospheres, which could be used to trace their formation origin. In this study, we quantify this effect in protoplanetary disks. We assume that the main nitrogen-bearing species are N_2 and NH_3, since other volatiles that contain nitrogen have significantly lower abundances in comparison (e.g., Mumma & Charnley 2011). We use the measured total nitrogen abundance in the Solar system, $n_N = 8 \times 10^{-5} n_H$ (Lodders 2003), where n_H is the hydrogen abundance in the disk midplane. Similarly to the case of CH_4 (see Section 3), we explore the parameter space of possible NH_3 abundances using data from the Spitzer c2d Legacy ice survey, as follows: (1) no NH_3, (2) the median NH_3 observed abundance $n_{NH_3-mid} = 0.055 \times n_{H_2O}$ (Öberg et al. 2011a), and (3) the maximum observed NH_3 abundance $n_{NH_3-max} = 0.1537 \times n_{H_2O}$ (Bottinelli et al. 2010). In each case, the N_2 abundance then simply follows as $n_{N_2} = (n_N - n_{NH_3})/2$. We determine the locations of the N_2 and NH_3 snowlines by balancing desorption with readsorption (Hollenbach et al. 2009), with N_2 and NH_3 pure ice binding energies of 767 K and 2965 K, respectively (Fayolle et al. 2016, Martín-Doménech et al. 2014).

Figure 4 shows the snowline locations of the main oxygen and nitrogen carriers and the N/O ratio in gas and dust as a function of semimajor axis in a static disk for our three choices of the NH_3 abundance. For comparison, the horizontal dashed line shows the average N/O ratio in the disk. As expected, the gaseous N/O ratio generally exhibits an increasing trend towards the outer disk as more oxygen gas is depleted, with small decreases between the NH_3 and CO_2 snowlines (by x% for NH_3-mid and by x% for NH_3-max, respectively) due to NH_3 freeze-out. More importantly, the gas-phase N/O ratio in the outer disk is enhanced by more than a factor of three compared to its average value. This enhancement is more pronounced than the C/O gas-phase enhancement of a factor of two in the outer disk (see Figure 2). The N/O ratio reaches particularly high values between

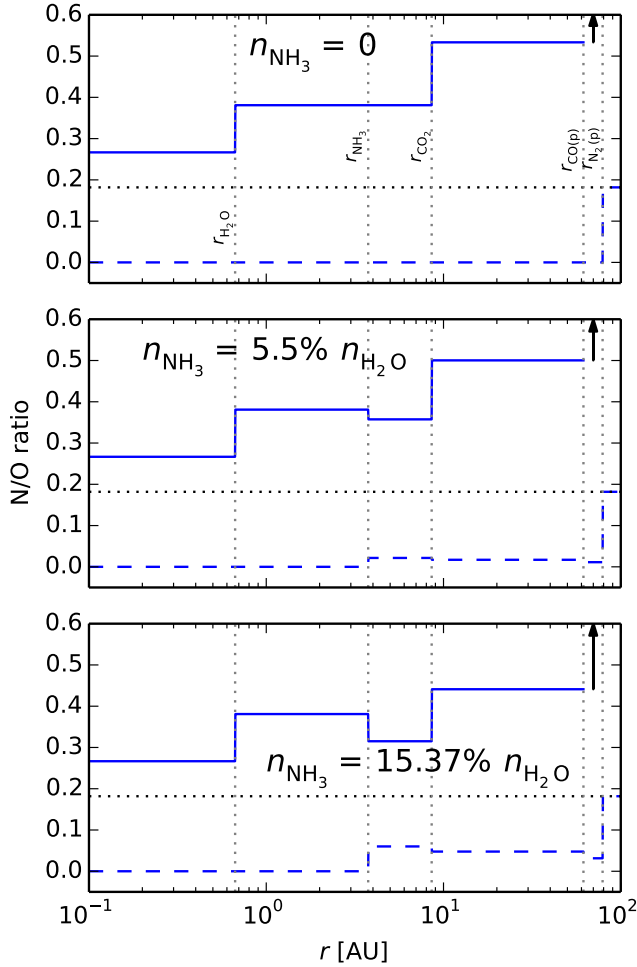the CO and N_2 snowlines, where all the oxygen is now contained in grains.

Fig. 4.— N/O ratio in a static disk for different NH3 abundances and N2 binding energies...

As is the case for CO, the N_2 binding energy is also strongly dependent on the ice environment in which it resides. If N_2 is layered on a water ice substrate, the N_2 binding energy is 1266 K (Fayolle et al. 2016). Figure 5 shows the H_2O, CO_2, CO and N_2 snowline locations in a viscous disk for particles with initial size ~ 0.06 cm $\lesssim s \lesssim 7$ m, and with the CO and N_2 snowlines calculated assuming different grain morphologies as explained above, as well as upper estimates for the N/O ratio in gas throughout the disk. The N_2 snowline moves inward by x% in the pure ice scenario and by x%....

5. DISCUSSION

Discuss how entrapment of volatiles by H2O affects volatile abundances and C/O ratios. Re-emphasize the fact that the C/O and N/O ratios are upper estimates, and that CH4 and NH3 might matter in a viscous disk. State that we plan to address this in a future paper. More TBD.
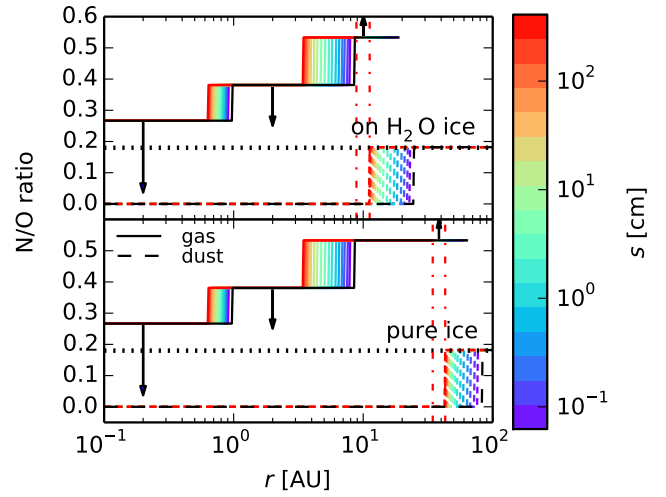
6. SUMMARY

Fig. 5.— N/O ratio as function of semimajor axis for N2 combined with H2O (top panel) and pure N2 ice (bottom panel).... Drift and gas accretion move the N2 snowlines inward by x% and y%, respectively. Overabundance of gas-phase N/O between the CO and N2 snowlines, marked by the vertical red dash-dotted lines for the largest drifting particles in our model.

Maybe we can include the summary in the discussion section?

REFERENCES

Andrews, S. M., Wilner, D. J., Hughes, A. M., Qi, C., & Dullemond, C. P. 2010, ApJ, 723, 1241
Birnstiel, T., Klahr, H., & Ercolano, B. 2012, A&A, 539, A148
Bottinelli, S., Boogert, A. C. A., Bouwman, J., et al. 2010, ApJ, 718, 1100
Chambers, J. E. 2009, ApJ, 705, 1206
Chiang, E., & Youdin, A. N. 2010, Annual Review of Earth and Planetary Sciences, 38, 493
Collings, M. P., Anderson, M. A., Chen, R., et al. 2004, MNRAS, 354, 1133
Cruikshank, D. P., Roush, T. L., Owen, T. C., et al. 1993, Science, 261, 742
Evans, II, N. J., Allen, L. E., Blake, G. A., et al. 2003, PASP, 115, 965
Fayolle, E. C., Balfe, J., Loomis, R., et al. 2016, ApJ, 816, L28
Fraser, H. J., Collings, M. P., McCoustra, M. R. S., & Williams, D. A. 2001, MNRAS, 327, 1165
Garrod, R. T., & Herbst, E. 2006, A&A, 457, 927
Hollenbach, D., Kaufman, M. J., Bergin, E. A., & Melnick, G. J. 2009, ApJ, 690, 1497

Kennedy, G. M., Kenyon, S. J., & Bromley, B. C. 2006, ApJ, 650, L139
Lodders, K. 2003, ApJ, 591, 1220
Martín-Doménech, R., Muñoz Caro, G. M., Bueno, J., & Goesmann, F. 2014, A&A, 564, A8
Mousis, O., Fletcher, L. N., Lebreton, J.-P., et al. 2014, Planet. Space Sci., 104, 29
Mumma, M. J., & Charnley, S. B. 2011, ARA&A, 49, 471
Mumma, M. J., Disanti, M. A., dello Russo, N., et al. 1996, Science, 272, 1310
Öberg, K. I., Boogert, A. C. A., Pontoppidan, K. M., et al. 2008, ApJ, 678, 1032
—. 2011a, ApJ, 740, 109
Öberg, K. I., Murray-Clay, R., & Bergin, E. A. 2011b, ApJ, 743, L16
Owen, T., Mahaffy, P. R., Niemann, H. B., Atreya, S., & Wong, M. 2001, ApJ, 553, L77
Owen, T. C., Roush, T. L., Cruikshank, D. P., et al. 1993, Science, 261, 745

Pérez, L. M., Carpenter, J. M., Chandler, C. J., et al. 2012, ApJ, 760, L17
Pontoppidan, K. M. 2006, A&A, 453, L47

Rodgers, S. D., & Charnley, S. B. 2002, MNRAS, 330, 660
Rubin, M., Altwegg, K., Balsiger, H., et al. 2015, Science, 348, 232
Shakura, N. I., & Sunyaev, R. A. 1973, A&A, 24, 337